RADIOXENON MEASUREMENTS WITH THE PHOSWATCH DETECTOR SYSTEM

Wolfgang Hennig[1], William K. Warburton[1], Anthony Fallu-Labruyere[1], Konstantin Sabourov[1], Matthew W. Cooper[2], Justin I. McIntyre[2], Anshel Gleyzer[3], Marc Bean[4], Ed P. Korpach[4], Kurt Ungar[4], Weihua Zhang[4], Pawel Mekarski[4], Rebecca M.Ward[5], Steven R. F. Biegalski[5], Derek A. Haas[2,5]

XIA LLC[1], Pacific Northwest National Laboratory[2], PhotoPeak, Inc[3], Radiation Protection Bureau, Health Canada[4], the University of Texas at Austin[5]

Sponsored by the National Nuclear Security Administration

Award No. DE-FG02-04ER84121

ABSTRACT

Many of the radioxenon detector systems used in the International Monitoring System (IMS) and in other applications employ beta/gamma coincidence detection to achieve high sensitivity. In these systems, the coincidence detection is implemented by requiring simultaneous signals from separate beta and gamma detectors. While very sensitive to small amounts of radioxenon, this approach requires careful calibration and gain matching of several detectors and photomultiplier tubes. An alternative approach is the use of a phoswich detector in which beta-gamma coincidences are detected by pulse shape analysis. The phoswich requires only a single photomultiplier tube and thus is easier to set up and calibrate, and can be assembled into a more compact and robust system.

In the past, we developed a COTS detector system, named PhosWatch, which consists of a CsI(Tl)/BC-404 phoswich detector, digital readout electronics, and on-board software to perform the pulse shape analysis. Several units of this system have now been manufactured and are currently being evaluated at several radioxenon research laboratories. In this paper, we will report results from production tests and some of the evaluations, including a side-by-side comparison of a SAUNA detector and a PhosWatch system using atmospheric radioxenon samples and a comparison of an ARSA-type detector and a PhosWatch system with samples made by irradiating stable xenon isotopes. In addition, we will show initial results obtained with a higher speed version of the readout electronics, digitizing at 500 MHz and thus able to better resolve the BC-404's fast pulses.

OBJECTIVES

The amount of radioactive xenon in the atmosphere is measured in several stations of the IMS established by the Comprehensive Nuclear-Test-Ban Treaty. Roughly half of these stations use a radioxenon detection system that employs beta/gamma detection, the Swedish Automatic Unit for Noble gas Acquisition (SAUNA; Ringbom et al., 2003); most of the other half use a high resolution gamma detection system with a germanium detector, the French SPALAX unit (Fontaine et al.,2004). In addition, several radioxenon research laboratories use the Automated Radioxenon Sampler and Analyzer (ARSA) or a beta/gamma well detector (BGW), both developed at Pacific Northwest National Laboratory (PNNL) (Reeder et al., 1998; Cooper, 2007a). The ARSA, SAUNA, and BGW all make use of beta/gamma coincidence to suppress background and achieve high sensitivity to the characteristic events from the radioxenon isotopes of interest, which emit beta particles or conversion electrons (CEs) in coincidence with gamma rays or X-rays.

While these systems are very sensitive to small amounts of radioxenon, their complex arrangement of separate beta and gamma detectors also requires careful calibration and gain matching, which can make them cumbersome to operate. An alternative approach is the use of a single phoswich detector (Ely, 2003; Hennig et al., 2006b; Farsoni et al., 2007) in which beta/gamma coincidences are detected by pulse shape analysis (PSA). We previously reported the development of a commercial off-the-shelf (COTS) radioxenon detector system consisting of a phoswich detector, readout electronics, and PSA software, named the PhosWatch (Hennig et al., 2008). The phoswich detector consists of a fast plastic scintillator cell containing the Xe gas and mainly absorbing beta particles and CEs, optically coupled to, and surrounded by, a slower CsI(Tl) scintillator mainly absorbing X-rays and gamma rays. It thus requires only a single photomultiplier tube (PMT) and electronics readout channel. Beta/gamma coincidences create characteristic “fast/slow” signals that can easily be distinguished from “slow only” or “fast only” non-coincident interactions by PSA algorithms implemented in the digital signal processor of the readout electronics, a DGF Pixie-4 module (Hennig et al., 2007b).

Having built a number of PhosWatch systems to commercial production standards, the objective of the work presented in this paper was to test and evaluate their performance in radioxenon monitoring applications, including comparisons to existing systems. All detectors were first tested and characterized at XIA for energy resolution and background. Then three PhosWatch systems were transferred to Health Canada, The University of Austin, and PNNL for evaluation. At Health Canada, the PhosWatch system is operated side by side with a SAUNA system using atmospheric radioxenon samples acquired with a SPALAX system. At The University of Austin, the PhosWatch system is operated in comparison to an ARSA-type system using radioxenon created by irradiating stable xenon isotopes in a local reactor. At PNNL, the PhosWatch system was tested with Xe and Rn samples. Further evaluation is still in progress at all three sites. Below we describe the results of these evaluations and in addition will show initial results obtained with a higher speed version of the readout electronics, digitizing at 500 MHz and thus able to better resolve the fast pulses from the BC-404.

RESEARCH ACCOMPLISHED

Production Tests at XIA

A total of 7 phoswich well detectors were built in a small-scale commercial production run and named PW3a-PW9. They all consist of a 1"-diameter BC-404 plastic cell with 2 mm wall thickness enclosed in, and optically coupled to, a 3" diameter, 3” tall CsI(Tl) cylinder in the geometry of the second prototype PW3 (Hennig et al., 2007a). (PW3a is the prototype PW3 rebuilt with a new PMT and crystal.) The PSA algorithms to separate beta/gamma coincidences from non-coincident interactions and to measure the energy deposited in the CsI (Ec) and in the BC-404 (Ep) have been described previously (Hennig et al, 2006a). Detectors were tested for vacuum tightness and typically leaked less than 1 Torr/h when evacuated to 1 Torr and disconnected from the pump.

Detectors were characterized by measuring resolutions at various energies with a number of test sources. As shown in Figure 2, the photon energy resolutions of PW3a-PW9 at medium to high photon energies are significantly better than resolutions reported for the ARSA detector (Reeder et al., 2004), and the later detectors (PW6-PW9), with improvements in detector assembly and careful selection of PMTs for low noise, reach an average ~7.3% FWHM at 662 keV. These later detectors thus match or exceed the resolutions reported for the BGW detector (Cooper, 2007a) in the preferred CsI(Na) variant and the SAUNA II detector. As summarized in Table 1, for low energy photons (Ec = 30 keV) and for CE from ^{131m}Xe (Ep = 129 keV), the phoswich detectors reach energy resolutions similar to

the other detector systems. Note that count rates and other experimental conditions can not be assumed to be the same for measurements performed at different times and institutions.

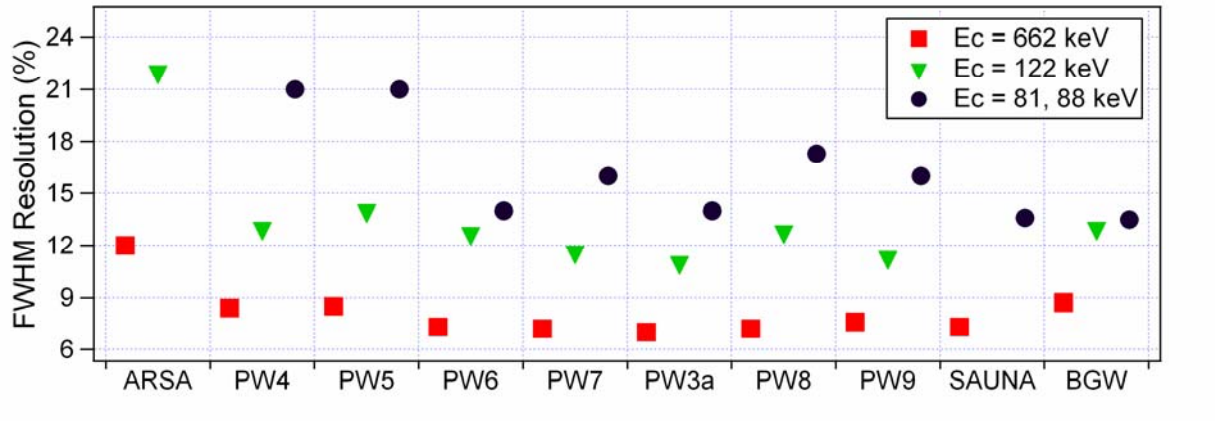

Figure 1. Resolution of photon energies for radioxenon detectors. Phoswich detectors are listed in order of production. The 81 and 88 keV data sets used internal ^{109}Cd and ^{133}Xe sources, respectively; other data sets used ^{137}Cs and ^{57}Co sources outside the detector. Non-phoswich data are from (Reeder, 2004; Cooper, 2007; Ringbom 2007), or measurements at Health Canada.

Table 1. Energy resolutions and background rates for radioxenon detection systems.

Detector system	**PhosWatch (typical values)**	**ARSA (Reeder, 2004; PNNL data)**	**SAUNA (A. Ringbom, 2007)**	**BGW (Cooper, 2007a; PNNL data)**
Resolution for 662 keV γ-rays	7.3%	12%	7.3%	8.7%
Resolution for 30 keV X-rays	28-35%	32%	23-30%	18%
Resolution for 129 keV CE	26-33%	25-30%	19%	25%
Background in lead enclosure (total)	3-8 counts/s	~30 counts/s (larger crystal)	7.5-12 counts/s	~5.5 counts/s
Background in lead enclosure (coincident)	0.02-0.08 counts/s	~0.1 counts/s	0.03-0.03 counts/s	~0.025 counts/s

In monitoring applications, the samples of radioxenon collected are very small, so the background count rate of the detector has to be as low as possible. In a lead enclosure (2" lead with 0.5" copper lining) we measure an overall rate of 3–8 counts/s for PW4–5 and PW8-9, of which ~0.02–0.08 counts/s are coincidences, and only ~0.002-0.004 counts/s fall in the ^{133}Xe regions of interest (ROIs) at 30 keV and 80 keV. PW6, PW7, and PW3a showed higher background rates (~10 counts/s total, ~0.5 counts/s coincident) due to small amounts of ^{40}K in the PMT and the CsI. This contamination has been eliminated for PW8 and PW9 by careful screening of crystals and PMTs before assembly. All detectors reject over 99% of radiation from an external ^{137}Cs source as non-coincident. Typical background rates for the larger ARSA detector and the similar sized SAUNA and BGW detectors are also listed in Table 1.

Evaluation at Health Canada and PNNL

As part of the evaluation of the PhosWatch system in monitoring application, Xe samples acquired with a SPALAX system were re-measured in parallel with PW5 and a SAUNA system at Health Canada. Figure 2 shows the number of coincidence events detected by PW5 in ROIs at Ec = 80 keV and Ec = 250 keV as a function of ^{133}Xe and ^{135}Xe

activity measured by the SPALAX system. While error bars must be assumed to be 10% or more due to uncertainties in the sample transfer, disregard of other isotopes, and simplifications in the correction for decay between measurements, the data shows a good linear correlation, indicating that PW5 results are consistent with the SPALAX results.

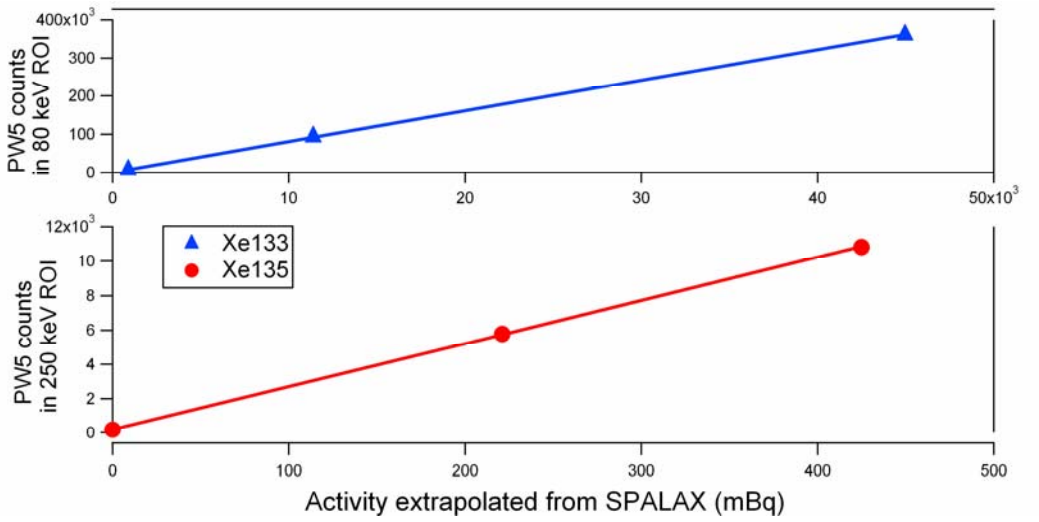

Figure 2. Counts in PW5 regions of interest vs. nominal activity from SPALAX measurement for several samples from a Canadian monitoring station.

Figures 3 and 4 show 2D and 1D energy spectra for a SPALAX sample divided between PW5 and a SAUNA detector. At the low photon energies of this sample, peak resolution is better for this SAUNA than for PW5 (the latter being one of our earlier phoswich detectors) but since the quantitative analysis only uses the number of counts in a ROI and peaks are well separated, the difference is not critical. In this and other measurements, we also observe that the background in PW5 is lower, and that the "memory effect" from Xe retained in the plastic from previous samples is about equal in this SAUNA and in PW5.

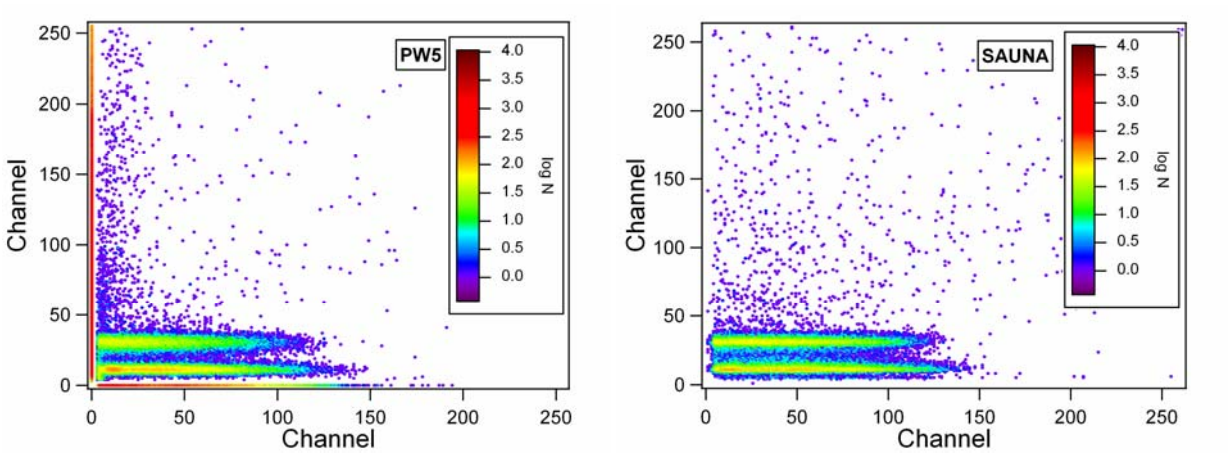

Figure 3. 2D histograms from a SPALAX sample split between PW5 (left) and SAUNA (right).

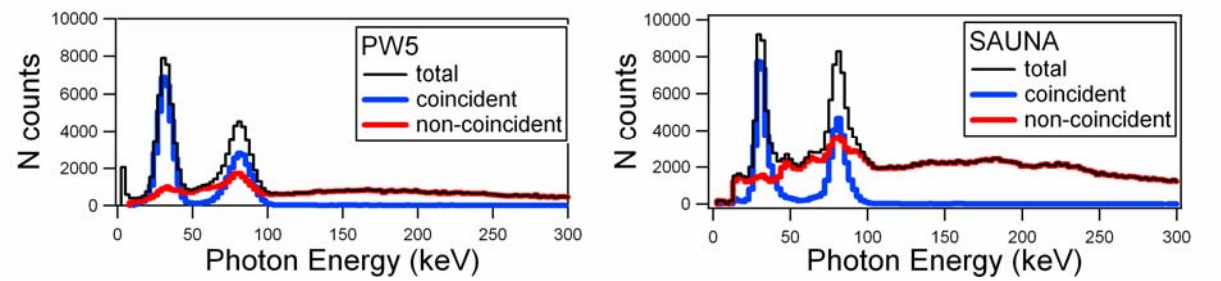

Figure 4. 1D spectra of photon energy for PW5 and SAUNA (data from Figure 3 projected to vertical axis).

To obtain a basis for quantitative analysis of PhosWatch spectra, the detector geometry was modeled with a Geant4 simulation, both for radiation processes and optical processes. We assumed the BC-404 cell to be filled with 15% xenon and 85% nitrogen, and used the following input parameters (besides literature constants): an outer reflectivity of 0.95, PMT quantum efficiency 30%, photocathode reflectivity 17%, signal risetimes (after a low pass Nyquist filter in the electronics) 100 ns for CsI, 13 ns for BC 404, and a coincidence time window for the PSA of 100 ns. We then compute the coincidence detection efficiency for each ROI as

$$\varepsilon_{\beta\gamma\_ROI} = \frac{C_{ROI}}{C_A \times BR_{ROI}} \qquad (1)$$

where C_{ROI} and C_A are the number of counts in the ROI and in total, respectively, and BR_{ROI} is the beta-gamma branching ratio for the ROI. To verify the simulation, we used the data in Figure 3 and a preceding background measurement to compute $\varepsilon_{\beta\gamma\_133Xe\_30}$ and $\varepsilon_{\beta\gamma\_133Xe\_80}$ from the product of gamma and beta efficiency, which are obtained from the ratios of coincident counts (in the ROI) and singles counts (projection of coincident and non-coincident events to beta or gamma axis). As shown in Figure 5, the simulated $\varepsilon_{\beta\gamma\_ROI}$ (x marks) agree well with the $\varepsilon_{\beta\gamma\_ROI}$ estimated from the data (solid circles). Also shown are $\varepsilon_{\beta\gamma\_ROI}$ given by the manufacturer for the SAUNA system at Health Canada (solid triangles) and phoswich $\varepsilon_{\beta\gamma\_ROI}$ derived from Xe and Rn measurements at PNNL (open symbols), using 98% detection efficiency for conversion electrons from ^{131m}Xe as the starting point for the method described in (Cooper, 2007b). Note that again experimental conditions and especially ROI boundaries may vary. In particular, in PNNL measurements, the Rn count rate was very low and backgrounds were high, leading to large uncertainties in the computed efficiency, which may explain the difference from the simulation. The most directly comparable efficiency between the different systems and methods may thus be $\varepsilon_{\beta\gamma\_131mXe}$, because with the clearly defined peak well away from the axes, the effects of ROI boundaries are minimal. This value is 79.8% from simulations, 81% from the PNNL measurements, and 57% for this SAUNA. Overall, we see that $\varepsilon_{\beta\gamma\_ROI}$ is significantly higher for PW5 than for this SAUNA, especially at low energy. One reason for the higher efficiency in the phoswich is that detection of low-energy X-rays is enhanced if they are in coincidence with a beta particle since the latter creates a large pulse in the PMT that is easy to trigger on.

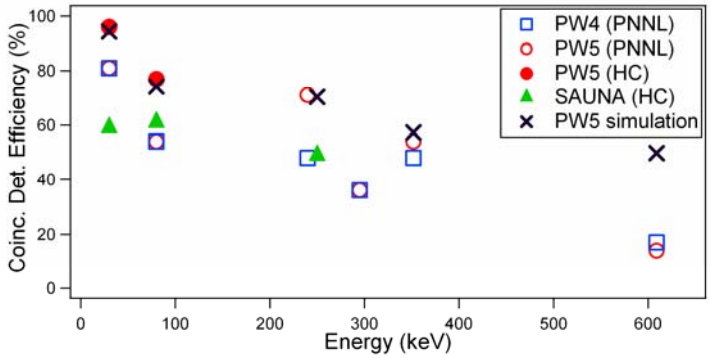

Figure 5. Coincidence detection efficiency of PW4, PW5 and a SAUNA detector installed at Health Canada. Values at 30 and 80 keV are from ^{133}Xe, not ^{131m}Xe or ^{222}Rn.

Using the simulated $\varepsilon_{\beta\gamma\_ROI}$ and a preceding background measurement for quantitative analysis of the PW5 data shown in Figure 5, we compute the concentrations of radioxenon isotopes shown in Table 2 (sample 1). We found 127 mBq/m^3 of ^{133}Xe in the sample at the time of the SPALAX measurement; concentrations for other isotopes were below 20 mBq/m^3. Computing the PW5 ^{133}Xe concentration separately for 6 ROIs that contain ^{133}Xe contributions showed variations from 122-129 mBq/m^3, indicating very good consistency within the PW5 measurement itself. The minimum detectable concentration (MDC) for this data is 0.5 mBq/m^3. Analysis of the SAUNA data taken in parallel to the PW5 measurement computed a ^{133}Xe concentration of 155 mBq/m^3 with an MDC of 0.2 mBq/m^3, and ROI variations from 145-168 mBq/m^3. The original SPALAX analysis measured a concentration of 194 mBq/m^3. (It has no comparable ROIs since it is not a beta/gamma coincidence system). In a second data set (sample 2), PW5 measured a ^{133}Xe concentration of 1274 mBq/m^3, the SAUNA measured 1486 mBq/m^3, and the SPALAX system measured 1873 mBq/m^3. We note that in both data sets, PW5 and SAUNA consistently measure ~65% and ~80% of the SPALAX values, respectively, and attribute this to the loss of sample volume during transfer and/or in the dead volume of the gas connections.

The MDC is derived from the standard deviation of background counts and interference between the ROIs in a particular measurement (Axelson, 2003) as the smallest activity detectable above background (at a 95% confidence level). By definition, it also depends on non-statistical factors such as the volume of air collected and the time since collection. The IMS requirement for ^{133}Xe is 1 mBq/m^3. Both systems, in both measurements, are well below this limit. In practice, the non-statistical factors are at least as important as the background factors; in particular, in the present case the volume is given by the SPALAX air collection and the split between SAUNA and PW5 (nominally 50% each). Since MDC and statistical uncertainties for the computed concentrations are small compared to the variations seen between ^{133}Xe ROIs as well as non-physical negative numbers presumed due to calibration issues, we consider the observed variations the most suitable measure of the precision of the measurements.

Table 2. Measured radioxenon concentrations in two samples acquired with SPALAX and re-measured with a SAUNA detector and with PW5. SAUNA and PW5 results include adjustments for decay since the SPALAX measurement. (The ^{135}Xe ROI was not fully contained in the spectrum in PW5 data.)

mBq/m^3		**SPALAX original sample**	**SAUNA re-measure ½ sample**			**PW5 re-measure ½ sample**		
Sample		**conc.**	**conc.**	**MDC**	**variation**	**conc.**	**MDC**	**variation**
1	**^{133}Xe**	194	156	0.2	145 -168	128	0.5	122 -129
	^{131m}Xe	5.8	1.3	1.6		4.4	1.4	
	^{133m}Xe	7.1	3.1	1.9		2.9	2.0	
	^{135}Xe	0	1.0	2.9		(1.0)	(3.3)	
	+/- error (all isotopes)	5-11**%**	<1			<1		
2	**^{133}Xe**	1873	1486	0.4	1380 -1691	1274	0.6	1208 -1288
	^{131m}Xe	14.1	-21.4	5.2		14	4.2	
	^{133m}Xe	108	55	6.0		50	6.3	
	^{135}Xe	806	788	3.8		(419)	(3.6)	
	+/- error (all isotopes)	--	1.5-8.3			1.3-5.3		

Evaluation at The University of Austin

In experiments at The University of Texas' Nuclear Engineering Teaching Laboratory, radioxenon gas was produced at by activating stable enriched xenon gas in the 1.0-MW TRIGA reactor. Samples were measured in PW6 and results were compared to equivalent measurements with an ARSA-type detector. Measurements were performed with all 4 isotopes; below we focus on the results from ^{135}Xe. Analysis and further measurements with other isotopes are in progress. To produce ^{135}Xe, ^{134}Xe was irradiated in the reactor and underwent a neutron capture

reaction. The stable gas is enriched to 99.61% ^{134}Xe. The sample used in the ARSA-type detector was irradiated in beam port 2 (BP2), which is tangential to the core. The gas samples used for PW6 were produced using in-core irradiation, irradiated in the lead-lined 3L facility, which lies within the 7L facility. Irradiation time and powers were adjusted to account for differences in fluxes and produce similar activities. The fluxes, irradiation times, and irradiation powers are listed for both irradiations in Table 3.

Table 3. Irradiation time, power and fluxes for measurements at The University of Texas.

Detector	Isotope	Power (kW)	Time	Flux (n/cm^2/s)
ARSA-type	Xe-134	950	8 h	1x10^8
PW6	Xe-134	100	15 min	1x10^{11}

The ARSA-type detector system used in this experiment contains two NaI crystals and four beta cells, like the ARSA system. The beta cells are inserted into holes in the NaI assembly. Each beta cell is connected to two PMTs, as is each gamma cell, for a total of 12 PMTs. The entire apparatus is cased in lead housing to reduce background from cosmic radiation. The data processing was done by NIM and CAMAC electronics. Gain matching was performed for the beta and gamma cells and the energy was calibrated using standard sources (Haas, 2008).

While the stable xenon gas that underwent irradiation was highly enriched in ^{134}Xe (99.61%), it still contains small quantities of the other xenon isotopes, most notably ^{132}Xe, which is present in 0.29% abundance. Thus these other isotopes are irradiated along with the ^{134}Xe, making the sample slightly impure. This impurity is augmented by the short-lived nature of ^{135}Xe, as it is the shortest lived of the radioisotopes with a half life of 9.14 hours. Consequently, the activity of ^{135}Xe only dominates the sample for approximately 4.5 days, at which point ^{133}Xe decay begins to dominate the sample activity. The computed activity of various isotopes of xenon over time is shown in Figure 6. Due to the transient nature of ^{135}Xe, data used in this experiment to characterize the detectors was taken from the first day of data collection to ensure that adequate ^{135}Xe was present.

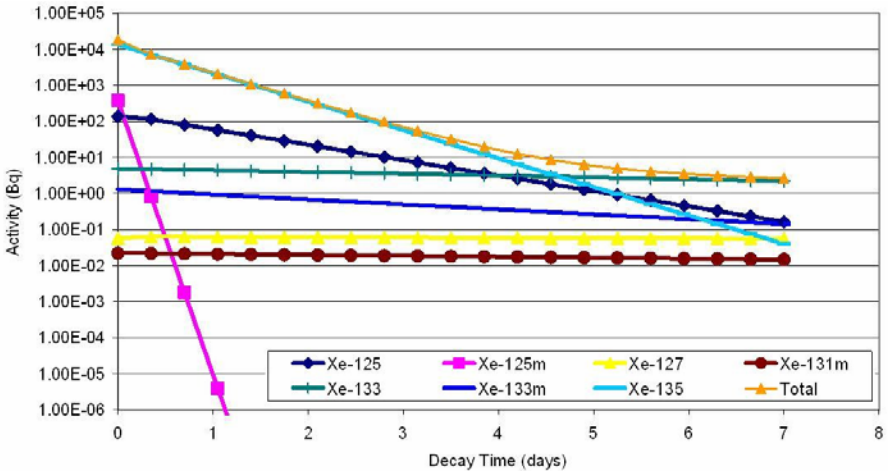

Figure 6. Activity contributions from radioxenon isotopes after irradiation of ^{134}Xe for 15 min at 100 kW.

To verify that the dominant isotope produced and detected in measurements with PW6 was, in fact, ^{135}Xe, a half-life measurement was made using the raw data. The count rate in the peak region was calculated at five points over the course of a day and plotted versus time. The resulting graph is presented in Figure 7. An exponential curve fit yields the equation shown on the graph, with a decay constant λ = 7.45x10-2 h^{-1}. This equates to a 9.31 h half-life, which is within 2% of the known half-life of ^{135}Xe, 9.14 h. Thus the count rate data collected by the phoswich detector confirms the dominant presence of ^{135}Xe with a high degree of accuracy.

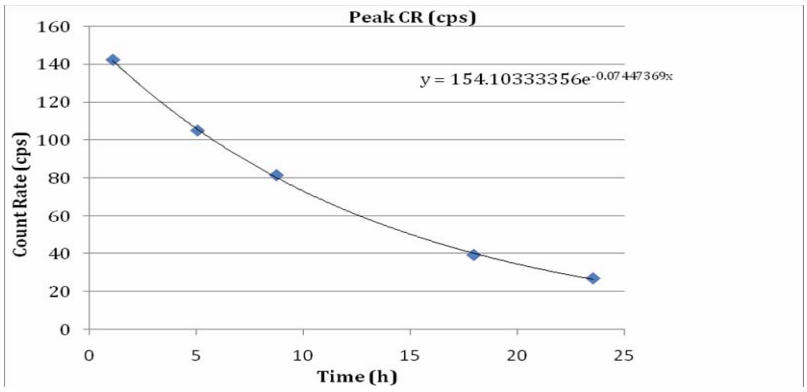

Figure 7. Count rate in PW6 measurement versus time, consistent with theoretical ^{135}Xe half-life.

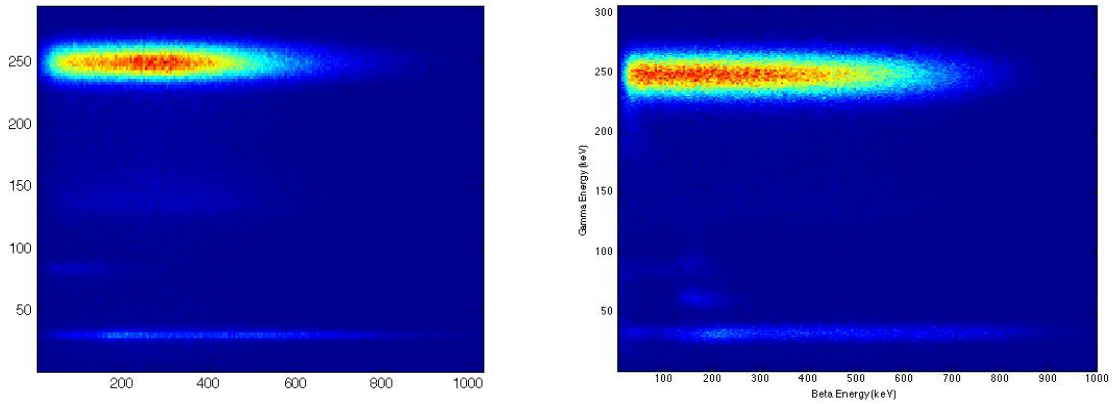

Figure 8. ^{135}Xe spectra from the ARSA-type detector (left) and PW6 (right). Axes are scaled in keV.

The ^{135}Xe spectra from both the ARSA-type detector and PW6 are shown in Figure 8. Both spectra feature the characteristic ^{135}Xe peak at Ec = 250 keV, and also show peaks at Ec = 81 and Ec = 30 keV. The 81 keV peak is a gamma peak from ^{133}Xe, while the 30 keV peak is an X-ray. The two spectra are comparable; however, notable differences do exist:

1) The 250 keV peak in the PW6 spectrum appears wider than the comparable peak in the ARSA spectrum. For PW6, the FWHM resolution is 12 % (30 keV), for the ARSA-type detector, the resolution is 9.6% (about 24 keV). The 81 keV gamma peak is also far narrower and clearer for the ARSA-type detector than for PW6.

2) The beta counts in the PW6 spectrum appear to be clustered at lower energies, and the tailing off of the beta distribution as the energy reaches a maximum (910 keV) is less dramatic, as well.

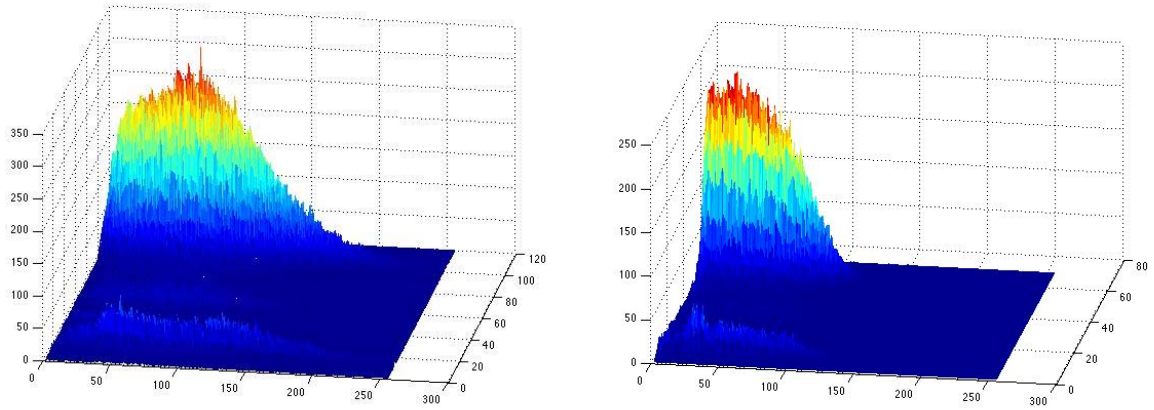

Figure 9. 3D surface plots of ^{135}Xe from ARSA-type detector (left) and PW6 (right). Axes are in channels.

The differing beta distributions between the two plots is even more evident in the surface plots, shown in Figure 9.The vertical axis is a measure of counts, while the x and y axis show beta and gamma channel, respectively. From these graphs it is clear that beta distribution is wider and tails off more slowly for the ARSA-type detector for both the 250 keV and 30 keV peaks, while the distribution for the phoswich detection rises and falls more sharply. The beta distributions for the 250 keV ROI (counts projected to the beta axis) and the theoretical distribution ("actual") are shown in Figure 10. The shape of the phoswich curve is very close to the theoretical distribution. The peak for the ARSA spectrum is at around 300 keV, which is higher than for the theoretical distribution and the PW6 spectrum. This difference in peak energy is due to the thinner wall of the plastic cell in the ARSA-type detector, which allows a portion of the high energy beta to deposit only a fraction of their energy in the plastic (effectively moving counts from high beta energy to lower beta energy).

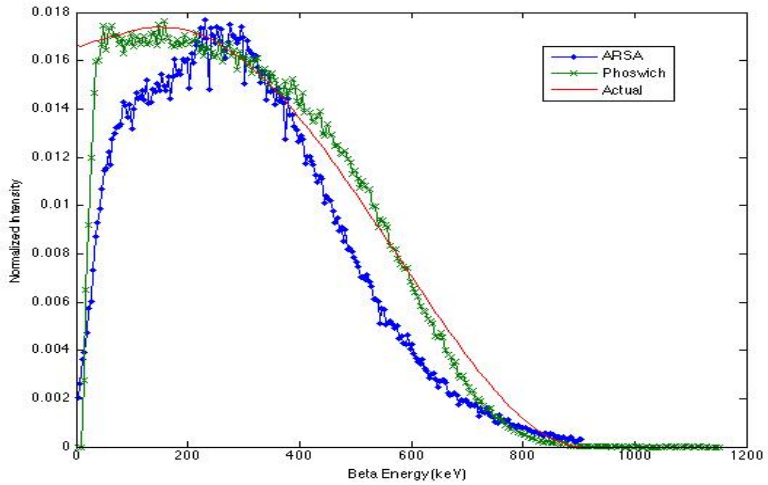

Figure 10. Theoretical, ARSA-type and PW6 beta distributions

Initial Results from 500 MHz Electronics

The DGF Pixie-4 used in the phoswich measurement digitizes the incoming detector signal at a rate of 75 MHz (13.3ns sampling) and this is sufficient to deliver good results in the PhosWatch system, as described above. Given the very fast pulses from the BC-404 (~2 ns decay time), it may however be beneficial to digitize the detector signal at a higher rate. As XIA is in the process of developing a Pixie-4 type module digitizing at 500 MHz, we used a prototype of this module, named P500, to explore possible improvements of the PhosWatch system with the higher speed electronics. In a preliminary test, a planar 1" CsI/BC-404 phoswich detector (PW1 from Hennig et al., 2006a)

was connected to a fast PMT (XP2020), irradiated with ^{137}Cs, and read out with a P500 and a Pixie-4. Detector waveforms were processed offline with the same PSA algorithms used in the standard measurements.

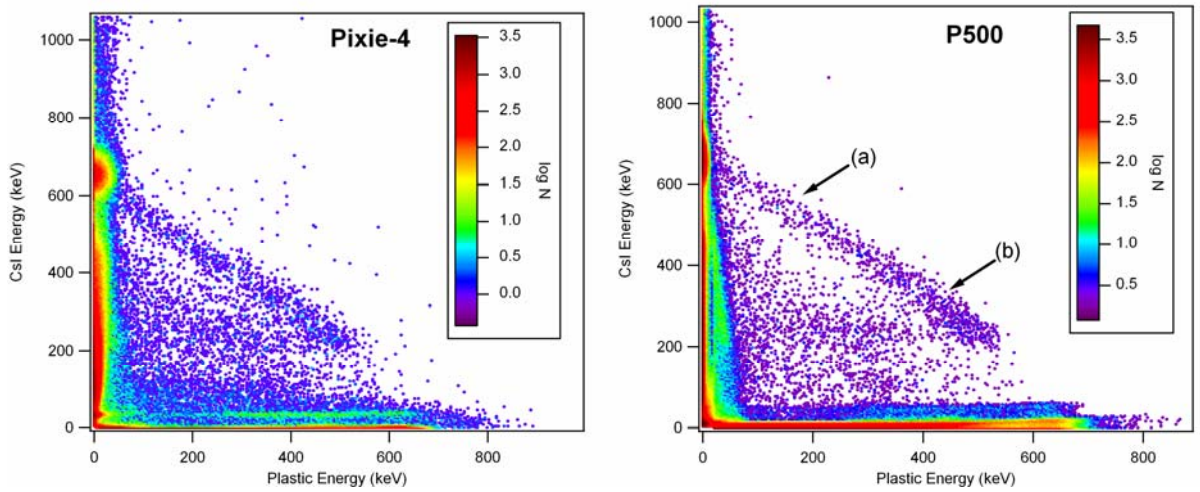

Figure 11. 2D energy histogram from PW1 computed offline from Pixie-4 and P500 waveforms. In contrast to Figure 3, non-coincident events are *not* contracted to the axes.

2D energy histograms of these measurements are shown in Figure 11. Both histograms show the typical features for ^{137}Cs measurements. Since in the planar geometry the source can be brought close to the BC-404, we can also detect the 624 keV CE from the second decay branch of ^{137}Cs, which is in coincidence with a ~30 keV X-ray. The main difference between the two systems is illustrated by looking at two events from the line of constant energy in detail: In each set of waveforms (a) and (b), as marked in Figure 11, the total energy deposited is ~662 keV, but in (a) only ~180 keV is deposited in the plastic while in (b) ~450 keV is deposited in the plastic. While in waveforms (a) there is almost no plastic contribution visible to the eye for the Pixie-4 waveform, the P500 waveform shows a distinct fast plastic spike.

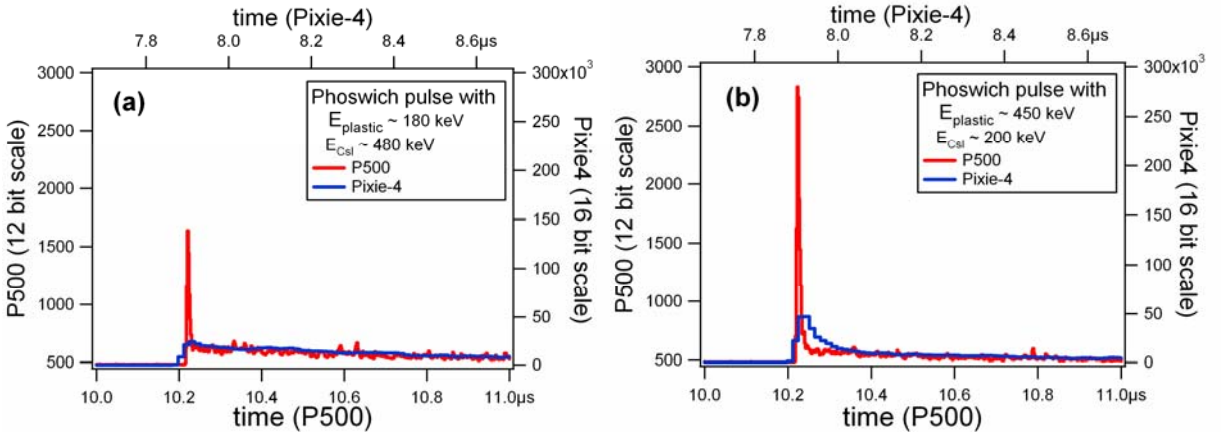

Figure 12. Phoswich waveforms captured by Pixie-4 and P500. The waveforms (a) and (b) are examples of events with energies falling into the Compton scatter line of constant energy at positions marked in Figure 11.

This better detection of the fast component translates directly in a better separation of event types. For example, part of the PSA calibration process includes measuring the slope formed by plotting the sum over the initial portion of the pulse (P) against the sum over the later portion of the pulse (C) for both plastic only and CsI only events. As shown in Figure 13, the slopes of the P vs. C distributions are much more "orthogonal" for the P500 than for the Pixie-4. Since the plastic contribution extends over so much less time in the P500, the length of P can be reduced from ~100ns to ~20ns, i.e. there is hardly any CsI contribution in P.

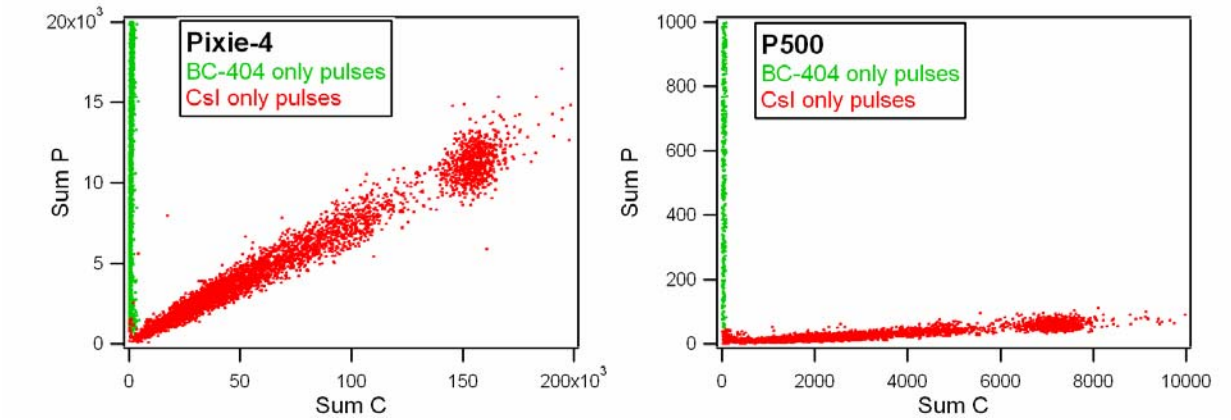

Figure 13. Scatter plots of P vs. C computed from phoswich waveforms. Axes are scaled to the same *ratio* for Pixie-4 and P500 plots.

In further characterization of the P500 system, we find that the energy resolution for the 624 keV CE is essentially equal (~14% FWHM), but resolutions are somewhat worse for 662 keV gamma rays (~10% for P500 vs. ~9.2% for Pixie-4 for this detector). In part, this can be attributed to the offline processing method, which omits the continuous baseline averaging implemented in online measurements that usually leads to improvements in resolution. Other factors may be the electronic noise in the system, which seems to particularly affect slow pulses and/or the precision of the Analog-to-Digital Converter (ADC) (12 bit for the P500 vs. 14 bit for the Pixie-4). We also find that the line of constant energy is slightly curved, similar to the behavior in some spectra reported from the SAUNA and BGW systems, and attribute that to the higher non-linearity associated with the fast ADC.

Future investigations in will include a closer look at reasons for increased noise, poorer linearity and degraded energy resolution. Also, for best results in this particular application, it may be beneficial to limit the P500 bandwidth, trading "orthogonality" of the scintillator contributions for more sampling points on the fast plastic spike and/or using the (pin compatible) 14bit, 400 MSPS ADC for better dynamic range and better linearity.

CONCLUSIONS AND RECOMMENDATIONS

In summary, we tested the PhosWatch radioxenon detector unit with standard test sources and with radioxenon samples from the atmosphere and from isotope irradiation. Overall, PhosWatch energy resolutions are comparable to existing systems, matching or exceeding resolutions at mid-high energies (~7.3% FWHM for 662 keV gamma rays for the later production batches) and reaching approximately 30% for both 30 keV energy X-rays and 129 keV CE. Background rates, memory effect, MDC, and coincidence detection efficiencies for the phoswich detectors are comparable to, and sometimes better than, values for existing systems. The phoswich detectors showed good consistency and precision in measurements with atmospheric samples, and produced comparable spectra in measurements with irradiated samples. The PhosWatch system also offers a significant advantage in ease of use and transportability. Since the design features only one PMT and does not depend on time coincidence, it eliminates the need for gain matching and – together with the compact electronics – greatly reduces the physical size of the detector, making it easier to deploy in the field. In future work, we will continue the side-by-side evaluations, and further explore performance improvements with the electronics digitizing at 500 MHz, which should allow even better detection of coincidences since fast plastic pulses are resolved better.

ACKNOWLEDGEMENTS

We thank A. Ringbom for helpful information about the SAUNA system gleaned through private communications.

REFERENCES

Axelson, A. and A. Ringbom (2003) Xenon air activity concentration analysis from coincidence data, FOI report FOI-R-0913-SE

Cooper, M. W., J. I. McIntyre, T. W. Bowyer, A. J. Carman, J. C. Hayes, T. R. Heimbigner, C. W. Hubbard, L. Lidey, K. E. Litke, S. J. Morris, M.D. Ripplinger, R. Suarez, and R. Thompson (2007a). Redesigned β-γ radioxenon detector, *Nuclear Instruments and Methods in Physics Research* A 579: 426–430.

Cooper, M.W., J. C. Hayes, T. R. Heimbigner, C. W. Hubbard, J. I. McIntyre, M. D. Ripplinger, and B. T. Schrom (2007b). Automated QA/QC check for β-γ coincidence detector, in *Proceedings of the 29th Monitoring Research Review: Ground Based Nuclear Explosion Monitoring Technologies*, LA-UR-07-5613, Vol. 2, pp. 739–746.

Ely, J. H., C. E. Aalseth, J. C. Hayes, T. R. Heimbigner, J. I. McIntyre, H. S. Miley, M. E. Panisko, and M. Ripplinger (2003). Novel Beta-Gamma coincidence measurements using phoswich detectors, in *Proceedings of the 25th Seismic Research Review—Nuclear Explosion Monitoring: Building the Knowledge Base*, LA-UR-06-6029, Vol. 1, pp. 533–541.

Farsoni, A.T., D.M. Hamby, K.D. Ropon, and S.E. Jones (2007). A two-channel phoswich detector for dual and triple coincidence measurements of radioxenon isotopes, in *Proceedings of the 29th Monitoring Research Review: Ground-Based Nuclear Explosion Monitoring Technologies*, LA-UR-07-5613, Vol. 2, pp. 747–756.

Fontaine, J.-P., F. Pointurier, X. Blanchard and T. Taffary (2004). Atmospheric xenon radioactive isotope monitoring, *Journal of Environmental Radioactivity* 72: 129–135

Haas, D.A., (2008). Producing beta-gamma Coincidence Spectra of Individual Radioxenon Isotopes for Improved Analysis of Nuclear Explosion Monitoring Data, Ph.D. dissertation, The University of Texas at Austin.

Hennig, W., H.Tan, W. K. Warburton, and J. I. McIntyre (2006a). Single channel beta-gamma coincidence detection of radioactive Xenon using digital pulse shape analysis of phoswich detector signals, *IEEE Transactions on Nuclear Science* 53: (2) 620.

Hennig, W., H.Tan, A. Fallu-Labruyere, W. K. Warburton, J. I. McIntyre and A. Gleyzer (2006b). Design of a phoswich well detector for radioxenon monitoring, in *Proceedings of the 28th Seismic Research Review: Ground Based Nuclear Explosion Monitoring Technologies*, LA-UR-06-5471, Vol. 2, pp. 801–810.

Hennig, W., H.Tan, A. Fallu-Labruyere, W. K. Warburton, J. I. McIntyre, and A. Gleyzer (2007a). Characterization of phoswich well detectors for radioxenon monitoring, in *Proceedings of the 29th Monitoring Research Review: Ground Based Nuclear Explosion Monitoring Technologies*, LA-UR-07-5613, Vol. 2, pp. 757–763.

Hennig, W., Y.X. Chu, H.Tan, A. Fallu-Labruyere, W. K. Warburton, and R. Grzywacz (2007b). The DGF Pixie-4 spectrometer – Compact Digital Readout Electronics for HPGe Clover Detectors, *Nuclear Instruments and Methods in Physics Research* B 263, 175–178.

Hennig, W., H. Tan, W. Warburton, A. Fallu-Labruyere, K. Sabourov, M. Cooper, J. McIntyre, and A. Gleyzer (2008). Development of a COTS Radioxenon Detector System Using Phoswich Detectors and Pulse Shape Analysis, in *Proceedings of the 30th Monitoring Research Review: Ground Based Nuclear Explosion Monitoring Technologies*, LA-UR-08-05261, Vol. 2, pp. 758–767

Reeder, P. L., T. W. Bowyer, and R. W. Perkins, (1998). Beta-gamma counting system for Xe fission products, *Journal of Radioanalytical and Nuclear Chemistry* 235: (1–2), 89–94.

Reeder, P. L., T. W. Bowyer, J. I. McIntyre, W. K. Pitts, A. Ringbom, and C. Johansson (2004). Gain calibration of coincidence spectrometer for automated radioxenon analysis, *Nuclear Instruments and Methods in Physics Research* A 521: 586–599.

Ringbom, A., T. Larson, A. Axelson, K. Elmgren, and C. Johansson (2003). SAUNA—a system for automatic sampling, processing and analysis of radioactive xenon, *Nuclear Instruments and Methods in Physics Research* A 508: 542–553.